Journal of Cleaner Production 429 (2023) 139277

Contents lists available at ScienceDirect

Journal of Cleaner Production

journal homepage: www.elsevier.com/locate/jclepro

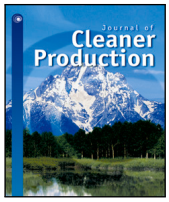

The impact of environmental conditions on the heat and emissions produced by large diesel engines in underground mines

Aaron Swift, Eric Smoorenburg, Alexandra Newman *, Gregory E. Bogin Jr.

Department of Mechanical Engineering, Colorado School of Mines, Golden, CO, 80401, USA

ARTICLE INFO

Handling Editor: Jing Meng

Keywords:
Underground mining
Heavy equipment
Heat
Emissions

ABSTRACT

Diesel-powered equipment generates significant heat and emissions in an underground mine. Studies in literature demonstrate that changes in ambient temperature and relative humidity affect engine performance and its emissions, which may in turn affect worker exposure. This study builds and simulates models of six Tier 2 turbocharged diesel engines, including aftertreatment systems, with displacement between 12.8 and 18.9 liters, to determine what, if any, feedback mechanism exists between local changes in temperature, pressure, and relative humidity, and the output of heat, nitrogen oxides, and soot from the engines. This study analyzes the simulation results under conditions representative of an actual mine, where measurements of 29°C, 80% relative humidity, and 103 kPa ambient pressure represent baseline conditions. After engines had operated for two hours, these same measurements were 37°C, 60% relative humidity, and 103 kPa ambient pressure. In the period between baseline and peak-temperature conditions, heat output increases up to 1.9% across all models, soot increases up to 5.2%, and nitrogen oxides decrease up to 16%. Results from this study can be used in a production scheduling optimization model to improve thermal management of the mine and to minimize heat-related disruptions in operations.

1. Introduction

Underground mining operations extract ore to support industries throughout the world. Mines are comprised of complex networks that can reach hundreds of meters beneath the surface (Widiatmojo et al., 2015). With several sources of heat in underground mines, the ventilation and refrigeration systems that maintain a safe working environment can be complex and costly, and as mines grow in size and depth, myriad factors that affect heat management must be considered (Sasmito et al., 2015).

Autocompression, strata, and electrical and diesel equipment are sources of heat in a mine; diesel equipment is also an emissions source (De la Vergne, 2014) and can account for more than 50% of the heat (Bascompta et al., 2016). These sources have a significant impact on ventilation requirements, refrigeration demand, and productivity. Health issues due to heat illnesses have been shown to cause loss of work days and a decrease in mine productivity (Michael Donoghue, 2004). A study following a small group of underground metal mine workers over seven days showed that workers' core temperatures could briefly exceed recommended limits while working in areas with a wet bulb temperature of up to 28.9°C (Yeoman et al., 2019). In a study examining heat strain on mine workers, performance was most significantly impacted for tasks requiring sustained attentiveness when workers were subjected to heat stress (Yeoman et al., 2022). Because of the hazardous conditions that can arise, the Mine Safety and Health Administration (MSHA) regulates mine ventilation plans in the United States (MSHA, 2023) to maintain a safe working environment. A study on diesel exhaust exposure in underground mines found that truck, load-haul-dump, and jumbo operators were among those with the highest exposure (Maximilien et al., 2017); however, the study did not consider how the ambient conditions affect emission characteristics of the equipment. The heat output from heavy diesel equipment within the confined spaces of an underground mine increases temperature near the equipment, which may, in turn, impact characteristics of the exhaust emissions. Greenhouse gas emissions can be attributed to mining operations (Norgate and Haque, 2010). More relevant to the nuisances this paper addresses, Paluchamy et al. (2021) provide a review of literature examining the effects of and mitigation strategies for airborne respirable dust in underground mines.

This study examines, for a static snapshot in time, how the heat and emissions outputs of turbocharged diesel engines are affected by their size and power rating under various environmental conditions; in the context of local changes to temperature, pressure, and relative humidity, this paper determines whether there are runaway effects, i.e., a feedback mechanism between the heat and emissions

* Corresponding author.
E-mail address: anewman@mines.edu (A. Newman).

https://doi.org/10.1016/j.jclepro.2023.139277
Received 31 March 2023; Received in revised form 6 October 2023; Accepted 11 October 2023
Available online 13 October 2023

characteristics and the increased local temperature caused by the equipment. The results can be used to generate input data for a production scheduling optimization model that includes constraints on the maximum heat load in working areas. The contribution of this paper is to simulate turbocharged engines with aftertreatment systems under environmental conditions, i.e., temperature, pressure, and relative humidity, expected in an underground hard rock mine by developing 1-D engine models in the GT-SUITE v2017 (Gamma Technologies, 2017) software package for six diesel engines used in mining applications. The size of the equipment, the fact that it is turbocharged and possesses aftertreatment systems, and that heat output (in addition to emissions) of the equipment is measured adds to existing literature. Results from the simulation are then analyzed alongside operational temperature data recorded in a mine to determine what changes can be expected over the course of a shift.

2. Background

Experimental studies have examined how engine performance and emissions are affected by pressure (Liu et al., 2014) and temperature (Pan et al., 2015). A recent study using a different engine simulation package examined the effect of both over a wider range of input parameters in addition to humidity (Ceballos et al., 2021), but the engine modeled was smaller (5.96L) and did not include turbocharging or aftertreatment, both of which are included here. An increase in the ambient temperature lowers the air density and the mass of air inducted into the cylinders, which alters both the power output and fuel consumption. It also results in an increase in the enthalpy carried in the exhaust gas (Abassi et al., 2010) and shortened ignition delay (Juva et al., 1989). A decrease in atmospheric pressure affects fuel consumption and soot production by reducing the amount of oxygen available for combustion; studies examining naturally aspirated engines (Liu et al., 2014; Ceballos et al., 2021) observe that an increase in ambient pressure is accompanied by a reduction in soot and fuel consumption. Increased humidity reduces the peak combustion temperature because water vapor has a higher specific heat capacity than air and can absorb more energy before increasing in temperature, which alters the emissions characteristics (Lin and Jeng, 1996). Results regarding the production of NO_x vary among the studies – Pan et al. (2015) and Ceballos et al. (2021) find that it increases with temperature and Lin and Jeng (1996) find that it decreases; the effect of humidity is similarly mixed – Lin and Jeng (1996) observe that NO_x decreases with humidity and Ceballos et al. (2021) find little effect. However, investigations into the implications on exhaust emissions and heat output of diesel engines in confined spaces, such as underground mines, are limited. This paper differs from aforementioned works by considering engines with aftertreatment systems: all models include a diesel oxidation catalyst, which lowers the emissions of CO, NO, and unburned hydrocarbons, and one model adds to that a diesel particulate filter that reduces soot. Additionally, the sizes of engines examined in this study – 12.8 to 18.9L – are larger than those in the previously mentioned studies, which range between 1.77 and 9.73L. The selection of engines also facilitates comparisons between (i) similarly sized engines with different power ratings, and (ii) engines with similar power ratings and different sizes.

Understanding the effects of environmental conditions on diesel equipment requires an understanding of the underlying concepts of heat transfer in an engine. Typical diesel engines have a brake thermal efficiency between 30 and 48%, primarily as a function of engine displacement (Breeze, 2018). Brake thermal efficiency reflects how much of the heat provided by the combusted fuel is converted to shaft power. The remaining fuel energy can be divided into heat losses, parasitic loads, and exhaust losses (Pulkrabek, 2004). In a typical diesel engine, 34% to 38% of fuel energy is converted to brake power, 22% to 35% is released to the environment as heat in the exhaust stream, 16% to 35% is transferred directly to the engine coolant before it is eventually dissipated to the environment through the radiator, 2% to 6% is rejected to the oil or the ambient environment via convection and radiation, and 1% to 2% is lost in incomplete combustion (Heywood, 1988).

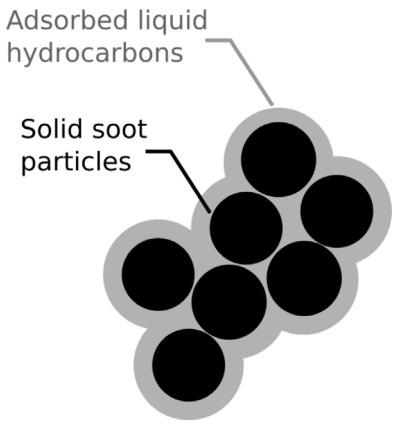

Fig. 1. A representation of diesel particulate matter, consisting of solid soot particles (black circles) and liquid hydrocarbons (gray circles) that have either adsorbed or condensed on the surface of the solids.

The heat released by the exhaust of an engine comes in two forms: latent and sensible. Sensible heat is measured using the dry-bulb temperature, and indicates changes in the air temperature. Latent heat is measured using the wet-bulb temperature and indicates changes in relative humidity. Wet-bulb temperature is the most common heat stress index in mining (Roghanchi and Kocsis, 2018) because it considers the effects of both temperature and humidity. The body's thermal regulation depends on the evaporation of sweat and how quickly it can be dissipated into the atmosphere (Hartman et al., 1997); as humidity increases, the cooling effect decreases due to the reduced rate of evaporation. Engines release latent heat in the form of water vapor, which has a direct impact on the local humidity: a liter of diesel fuel consumed in an engine produces approximately 1.1 liters of liquid water vapor in the exhaust gas (Maurya et al., 2015).

Diesel exhaust from the tailpipe carries both particulate and gaseous emissions, specifically soot, unburned hydrocarbons, and NO_x. Soot consists of solid carbon particles that are produced in fuel-rich regions within the combustion chamber. It is a component of diesel particulate matter (DPM, see Fig. 1), the characteristic black smoke visible in exhaust, which is formed when solid soot particles combine with liquid hydrocarbons and other solid materials that remain after the combustion process; the resulting particles pose a health risk because they are small enough to become trapped in the lungs when inhaled (Mohankumar and Senthilkumar, 2017). Unburned hydrocarbons in the exhaust are the remains of unburned fuel, partially oxidized reaction products, and the fuel molecules that have decomposed due to high temperatures (Turns, 2012). Some of these species are further oxidized in the diesel oxidation catalyst (DOC), decreasing their concentration in the exhaust gas, but any unreacted hydrocarbons exit the tailpipe. NO_x is comprised of nitrogen oxides, typically NO, formed through the high-temperature Zeldovich mechanism, the most prevalent among four NO_x formation mechanisms. The oxidation of nitrogen increases under high-temperature conditions, causing the nitrogen in the air to dissociate and react with oxygen, producing NO_x (Lakshminarayanan and Aghav, 2010). Some of the NO formed at high temperature may be oxidized into NO_2 in relatively low-temperature regions by reacting with HO_2 radicals (Turns, 2012). Exposure to NO_2 can result in adverse respiratory effects such as pulmonary inflammation or exacerbation of asthma (EPA, 2016).

3. Methods and validation

This study develops one-dimensional models in GT-SUITE for the engines used in the following mining vehicles: Atlas Copco MT6020

Table 1
Parameters for the engines in this study. All models are turbocharged and include a diesel oxidation catalyst (DOC) for aftertreatment; the C15 adds to this a diesel particulate filter (DPF). References: 1: Nogva (0000) 2: Volvo Penta (2013d) 3: Volvo Penta (2013c) 4: Caterpillar (2019) 5: Volvo Penta (2013b) 6: Volvo Penta (2013a).

Engine model	Trucks			Loaders		
	MT6020	TH663	TH540	R2900G	LH621	LH514
	Cummins QSK19-C760	Volvo TAD1643VE-B	Volvo TAD1640VE	Cat C15 ACERT	Volvo TAD1344VE	Volvo TAD1340VE
Bore (mm)	159	144	144	137.2	131	131
Stroke (mm)	159	165	165	171.5	158	158
Displacement (L)	18.9	16.1	16.1	15.2	12.8	12.8
Power output (kW)	567	565	405	321	352	256
Torque output (N-m)	3084	3261	2761	2055	2215	1770
Number of cylinders	6	6	6	6	6	6
Compression ratio	15:1	17.5:1	17.5:1	18.0:1	18.1:1	18.1:1
Emissions category	Tier 2	Tier 2	Tier 2	Tier 3	Tier 2	Tier 2
Emissions equipment	DOC	DOC	DOC	DOC, DPF	DOC	DOC
Reference	1	2	3	4	5	6

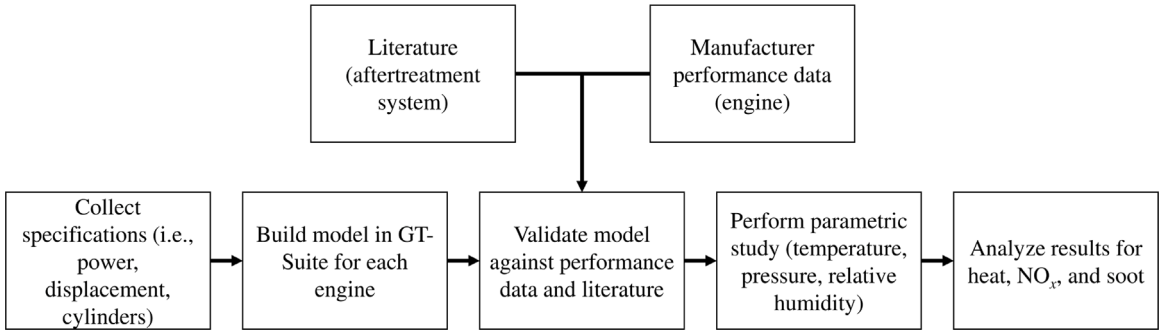

Fig. 2. A block diagram depicting the process used to conduct this study.

(Cummins QSK19-760 engine), Sandvik TH663 (Volvo TAD1643VE-B), Sandvik TH540 (Volvo TAD1640VE), Cat R2900G (Cat C15 ACERT), Sandvik LH621 (Volvo TAD1344VE), and the Sandvik LH514 (Volvo TAD1340VE). The procedure employed is as follows: (i) gather specifications regarding each vehicle, engine, and aftertreatment system, (ii) build a model in GT-Suite, (iii) validate each engine model against manufacturer performance data at 25°C, 100 kPa, and 50% relative humidity, (iv) upon successful validation, conduct a parametric study of various temperature, pressure, and relative humidity inputs, and (v) collect and analyze the results. Each model is built and validated using published information from the engine manufacturer. Key engine parameters are given in Table 1. After each model is validated against the published power, torque, and fuel consumption across a range of operating speeds, it is then used in a parametric study in which the ambient temperature, pressure, and relative humidity are varied to observe the effects on the heat and emissions output in the exhaust. Fig. 2 illustrates the process.

Fig. 3 shows a model representing the Volvo TAD1344VE, comprised of the engine and controls, including the turbocharger, intercooler, intake and exhaust manifolds, fuel injectors, and proportional–integral–derivative (PID) feedback fuel controller, which adjusts the mass of fuel injected per cycle to produce a target power output at the crankshaft. Parameters such as the bore, stroke and compression ratio were taken from manufacturer specifications and are listed in Table 1. Information not available in the manufacturer data such as the intake and exhaust valve size and lift were estimated based on literature (Jääskeläinen and Khair, 2018; Heywood, 1988), or automotive parts catalogs (Heavy Duty Pros, 0000a,b) to ensure model accuracy.

Start-of-injection timing for the fuel is fixed, with the PID fuel controller injecting the mass of fuel required to maintain target power. The fuel controller varies the discharge coefficient of the fuel injector, with the start of injection, end of injection, and injection pressure remaining constant. Air pressure in the intake manifold is regulated by a wastegate controller on the turbocharger. To ensure that the model arrives at a steady-state solution, each engine is simulated for 100 cycles, at fixed ambient conditions of 25°C, 100 kPa, and 50% relative humidity with engine speeds between 800 RPM (an approximate idle speed) and the maximum engine speed (typically between 1900 and 2100 RPM) in 200-RPM increments. Those outputs are then compared against charts in the manufacturer specifications for power, torque, and brake-specific fuel consumption; Fig. 4 depicts the results. At 1800 RPM, the engine speed used in the parametric study, power and torque are within 1% for all models; brake-specific fuel consumption is within 14%, on average, and 22% in the worst case. Across all models and engine speeds, power, torque, and brake-specific fuel consumption are, respectively, within 5%, 5%, and 13%, on average, and 32%, 32% and 31%, at worst. Results for the remaining two engines are listed in Tables 2 and 3 due to data being available at only a single engine speed.

GT-Suite solves the Navier–Stokes equations to obtain the flow through the model. This model employs an explicit solver to integrate the continuity, momentum, and energy conservation equations over time in the direction of flow. The software automatically determines the timestep based on the fluid velocity and the discretization length in the flow elements. A complete "flow circuit" from the air intake to the exhaust is solved for the flow velocity and temperature. Fig. 3 shows the schematic for the Sandvik LH621 underground loader. The arrows in the figure trace the flow from the ambient air, IntAmbient, through the compressor, intercooler, and intake manifold where it separates between the cylinders. Air then flows into each cylinder through the intake valves, is combusted with the fuel, and then travels out of the cylinder through the exhaust valves, into the exhaust manifold, through the turbine, the diesel oxidation catalyst, and out to the environment. There are two copies of the diesel oxidation catalyst subassembly in the model: the top one solves for the fluid velocity and the bottom one solves for the species concentrations and temperatures.

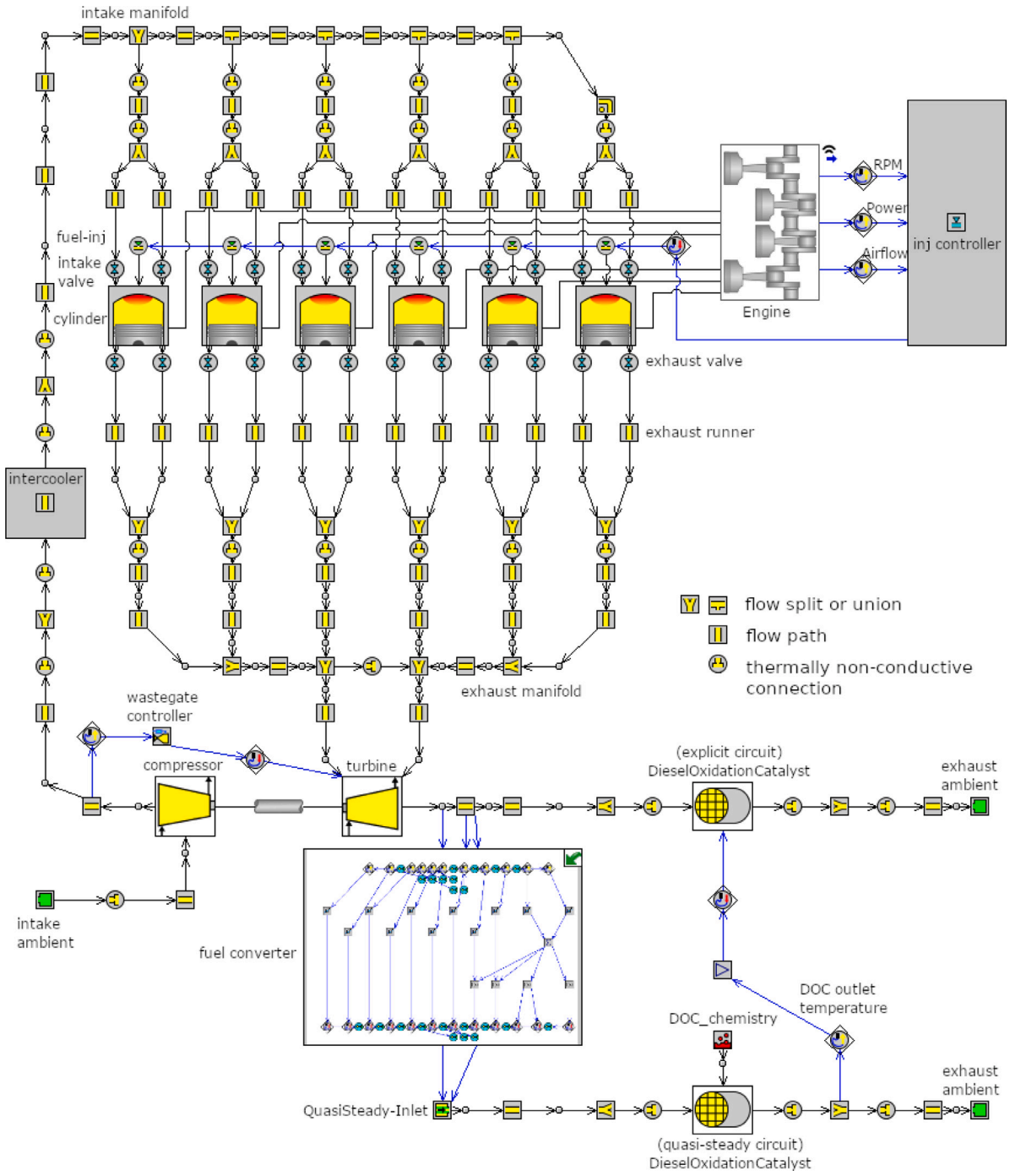

Fig. 3. GT-SUITE engine map of the Volvo TAD1344VE, a turbocharged 6-cylinder 12.8L diesel engine producing 352 kW peak power.

Table 2
Output of the QSK19-C760 model compared to engine manufacturer data. Fuel consumption was not available from the manufacturer, so values from two similarly sized generators from the same manufacturer are noted, along with the corresponding engine output: the QSK19-G4 (Cummins, 2019) and the KTA19-G4 (Cummins, 2020).

	1500 RPM		1800 RPM	
	Simulated	Actual	Simulated	Actual
Power (kW)	477	477	566	565
Torque (Nm)	3037	3037	3003	2997
Fuel Consumption (L/hr)	121	147 (QSK19-G4, 431 kW) 121 (KTA19-G4, 504 kW)	153	143 (QSK19-G4, 559 kW) 136 (KTA19-G4, 563 kW)

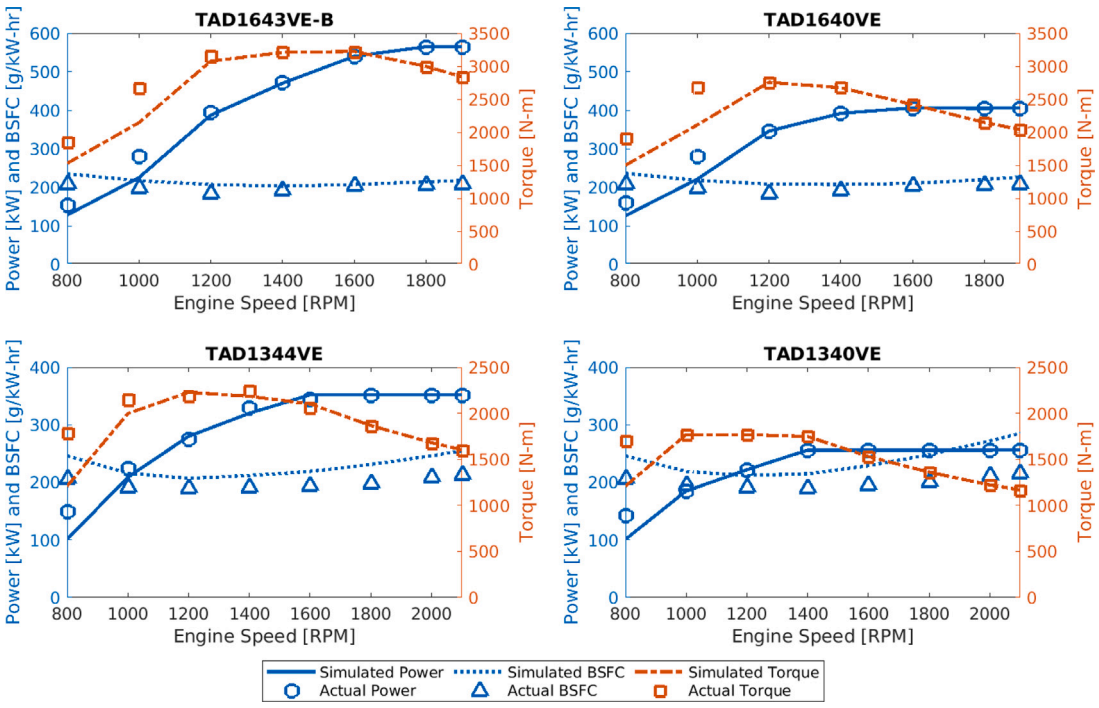

Fig. 4. Simulation output of each model at 25°C, 100 kPa, and 50% relative humidity compared to the published manufacturer data to validate model performance. BSFC: Brake-specific fuel consumption.

Table 3
Output of the C15 model compared to the engine manufacturer data. Values noted are from Wagner Equipment Co..

	1800 RPM	
	Simulated	Actual
Power (kW)	321	321
Torque (Nm)	1702	1702
Fuel Consumption (g/kW-hr)	232	198

The PID fuel controller, inj_controller, senses the engine speed, power, and airflow, then adjusts the fuel delivered by each fuel injector to achieve a target power output. The lower right portion of the figure depicts a duplicate of the aftertreatment system that uses a quasi-steady-state solver in a separate flow circuit to generate the chemical kinetics in the diesel oxidation catalyst and diesel particulate filter. In the solver, the mass flow rate is imposed and the resulting pressure is calculated. The large sub-assembly between the two imposes the mass flow rate, species concentrations, and temperature as boundary conditions for the aftertreatment circuit; the resulting diesel oxidation catalyst outlet temperature is then returned to the explicit circuit. Exhaust species concentrations are recorded from the outlet of the aftertreatment circuit. The use of separate solvers allows the two flow circuits to operate at different timesteps: the explicit circuit operates on the time scale of approximately one degree of crankshaft rotation, whereas the aftertreatment circuit has relatively larger timesteps for the chemical kinetics in the aftertreatment system.

The diesel oxidation catalyst employs the kinetic mechanism developed by Sampara et al. (2008a) for oxidation of CO into CO_2, oxidation of NO into NO_2, and oxidation of hydrocarbons into CO_2 and H_2O. Hydrocarbons in the exhaust are represented as a 50-50 split between propylene (C_3H_6) for partially oxidized fuel, and diesel ($C_{13.5}H_{23.6}$) for unburned fuel. The subassembly upstream of the aftertreatment circuit handles the conversion. The substrate of the diesel oxidation catalyst is a ceramic matrix with 400 cells per square inch, and the assembly was sized so that the gas hourly space velocity was approximately 60,000hr^{-1} based on the values given in Knafl et al. (2006) and Sampara et al. (2008b). The diesel particulate filter on the C15 uses a ceramic substrate with 200 cells per square inch and is sized to be the same diameter as the diesel oxidation catalyst (Dou, 2012). Due to the inclusion of the particulate filter in this model, it was also used to calibrate the NO_x and soot submodels against experimental emissions data taken for a 12-liter, 6-cylinder diesel engine with a diesel particulate filter and diesel oxidation catalyst (Zhu et al., 2011). Fig. 4 demonstrates the details of the validation.

4. Results and discussion

Using the validated engine models, this study simulates the engines at 1800 RPM, which aligns with the maximum power observed for each engine. The independent effects of pressure, temperature, and humidity on heat, soot, and NO_x emissions were determined by holding two parameters constant and varying the third. Temperature is examined from 25°C to 37°C in 2°C increments, pressure from 98 kPa to 107 kPa in 3 kPa increments, and relative humidity from 10% to 90% in 20% increments based on a mine operated by an industry partner. Air temperatures span from the median surface temperature (25°C) to the temperature at the lowest level (37°C) based on the contribution of autocompression and the virgin rock temperature as the air is delivered from the surface. Pressure varies to cover the change in elevation of the mine, and the range of humidity values is taken from observed values in meteorological data: 10% to 90%. The lowest wet-bulb temperatures associated with this range of environmental conditions is 10°C, corresponding to 25°C dry-bulb, 98 kPa, and 10% relative humidity; the highest wet-bulb temperature is 35°C, corresponding to 37°C dry-bulb, 107 kPa, and 90% relative humidity.

The air enters the compressor side of the turbocharger at ambient temperature and pressure; the air that enters the engine is at a higher pressure and temperature relative to the ambient conditions. Fuel also enters the engine at ambient conditions, so the only energy input is from the chemical energy in the reacted portion of the fuel. That portion is a function of the engine's combustion efficiency, which is observed to be above 99% in the simulation, with the unreacted portion leaving in the exhaust gas. The heat released from the exhaust gas

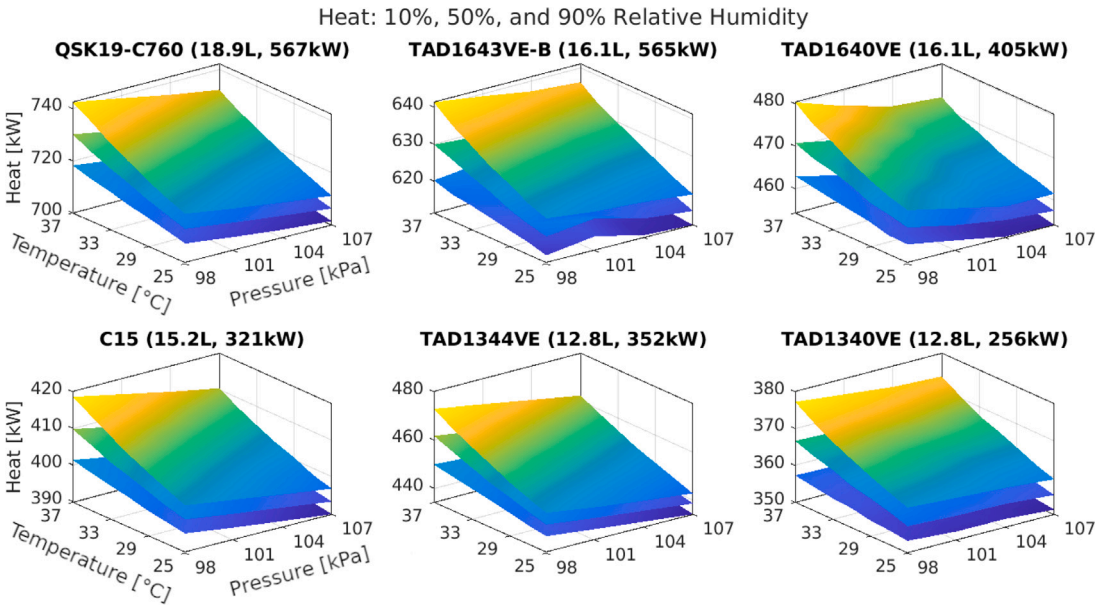

Fig. 5. Simulation results for each of the six engines depicted on each graph as one of three surfaces. Shown are heat outputs at 10% relative humidity (bottom surface), 50% relative humidity (middle surface), and 90% relative humidity (top surface). Note that the scale on the vertical axis varies between graphs to better differentiate relative humidity values.

includes the energy due to its elevated temperature, referred to as sensible heat, and the energy in the water vapor due to it being in a gaseous state as it leaves the engine, referred to as latent heat. Power from the engine is a function of the energy provided by the chemical reaction of the fuel $\dot{E}_{fuel}$ minus any unburned fuel $\dot{E}_{unburned}$, heat lost from the cylinder to the cooling fluid and oil $\dot{Q}_{cyl}$, mechanical energy lost to friction $\dot{W}_{fric}$, and the residual heat in the exhaust products $\dot{Q}_{exh}$, as shown in Eq. (1). Regarding the penultimate term of this equation, it computes mechanical friction based on recommended parameter values from GT-Suite documentation (Gamma Technologies, 2017) and from the software itself; the Chen-Flynn friction model (Chen and Flynn, 1965) determines friction mean effective pressure, which, in turn, yields the power lost to friction. Eq. (2) provides the power lost in the unburned fuel $\dot{E}_{unburned}$: the product of the mass flow rate and the enthalpy of the unburned hydrocarbons, $\dot{m}_{HC} \cdot \Delta h_{R,HC}$, which is added to the product of the mass flow and enthalpy of the carbon monoxide, $\dot{m}_{CO} \cdot \Delta h_{R,CO}$. These two species represent lost power because they can participate in a reaction to recover energy. To determine the heat released to the environment, Eq. (1) is re-arranged for the exhaust term, as shown in Eq. (3).

$$\dot{W}_{brake} = \dot{E}_{fuel} - \dot{E}_{unburned} - \dot{Q}_{cyl} - \dot{W}_{fric} - \dot{Q}_{exh} \quad (1)$$

$$\dot{E}_{unburned} = \dot{m}_{HC} \cdot \Delta h_{R,HC} + \dot{m}_{CO} \cdot \Delta h_{R,CO} \quad (2)$$

Re-arranging Eq. (1) to determine rate of heat output in the exhaust produces Eq. (3).

$$\dot{Q}_{exh} = \dot{E}_{fuel} - \dot{E}_{unburned} - \dot{Q}_{cyl} - \dot{W}_{fric} - \dot{W}_{brake} \quad (3)$$

Input values are given in Table 4 and corresponding simulation results for heat are shown in Fig. 5. Increasing either the air temperature or the relative humidity with the other parameters fixed results in an increase in heat output. By contrast, increasing only the pressure results in lower heat output. As the temperature rises from 25 to 37°C, a 4.1% increase on an absolute temperature scale, the air density decreases by 4.3% and the mass of inducted air also decreases by 2.8% (all numbers noted are from the TAD1643VE-B model). To maintain the specified power, 0.9% more fuel is injected into the cylinder, which lowers the air-to-fuel ratio by 3.5% and moves it closer to stoichiometric. The higher intake temperature also results in 1.6% higher peak combustion temperatures and higher exhaust temperatures. Increasing the pressure

Table 4
Parameters used to calculate heat output.

Parameter	Description	Units
$\dot{Q}_{exh}$	Rate of heat released in engine exhaust	kW
$\dot{E}_{fuel}$	Fuel power delivered to cylinder	kW
$\dot{E}_{unburned}$	Power from unburned fuel	kW
$\dot{Q}_{cyl}$	Rate of heat loss to cylinder walls	kW
$\dot{W}_{fric}$	Power lost to friction	kW
$\dot{W}_{brake}$	Brake power output	kW
$\dot{m}_{HC}$	Mass flowrate of unburned fuel	kg/s
$\dot{m}_{CO}$	Mass flowrate of carbon monoxide	kg/s
$\Delta h_{R,HC}$	Enthalpy of unburned fuel	kJ/kg
$\Delta h_{R,CO}$	Enthalpy of unburned carbon monoxide	kJ/kg

only results in a lower heat output due to reduced fuel required. For example, the 9% increase in pressure results in a higher air density, an 8.8% decrease in the pressure ratio across the compressor, and a 1.4% decrease in the temperature after the intercooler; the pressure in the intake manifold is relatively the same because of the wastegate controller; the net result is a 1.1% increase in the mass of air in the cylinder. The amount of injected fuel is relatively unchanged, decreasing by 0.3%, which increases the air-to-fuel ratio by 1.4% (owing to more lean combustion) and reduces peak cylinder temperatures by 0.7%. Increasing only the relative humidity results in a higher heat output due to increased fuel delivery to counteract the displaced oxygen and increased specific heat capacity of the intake air. The peak temperature decreases by 0.7%, but the mass of fuel injected increases by 0.5% to maintain the specified power, resulting in a 1.6% increase in exhaust enthalpy.

Fig. 6 illustrates the impact of ambient conditions on soot emissions. Soot production increases as either the humidity or temperature increases. The higher soot output in high-humidity cases is due to the added water vapor, which increases the specific heat capacity of the intake air. This causes a reduction in peak combustion temperature for the same amount of fuel delivered. In this case, the increased humidity causes 0.5% more fuel to be injected, resulting in a 0.7% decrease in peak combustion temperature and a 5.8% increase in soot production. Increasing the temperature leads to higher soot production due to the additional fuel required to counteract the effect of the lower air density. The temperature increase results in a 0.9% increase in the fuel injected

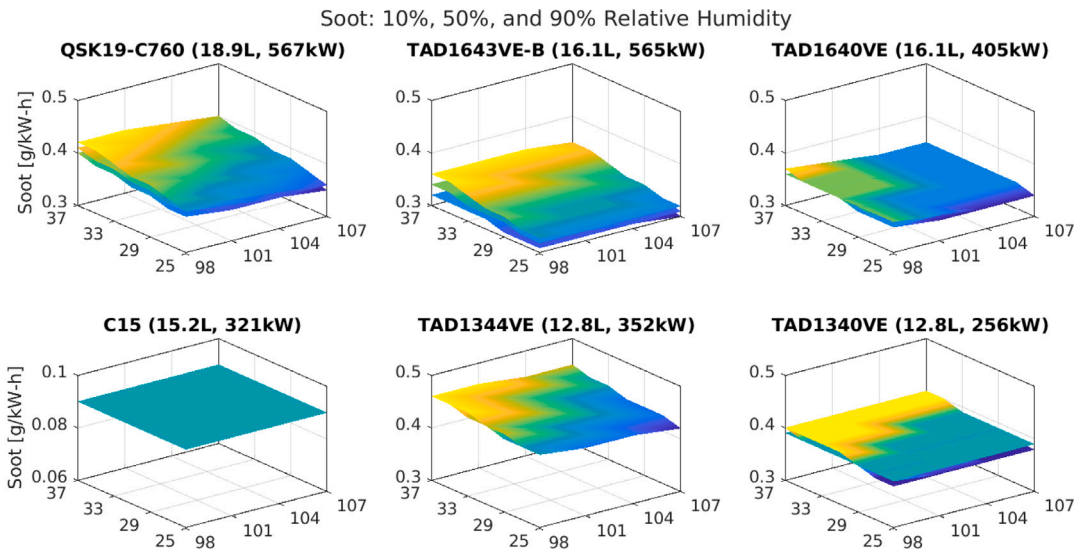

Fig. 6. Simulation results for each of the six engines depicted on each graph as one of three surfaces. Shown are soot outputs at 10% relative humidity (bottom surface), 50% relative humidity (middle surface), and 90% relative humidity (top surface). Note that the scale on the vertical axis for the C15 is lower due to the much lower soot output owing to the added particulate filter.

and a 2.8% decrease in the mass of air in the cylinder, resulting in a 3.5% decrease in the air-to-fuel ratio and 4.9% more soot. Increased pressure causes soot output to decrease by 1.6% because the increased ambient pressure leads to 1.1% more air in the cylinder. The amount of fuel required to maintain power decreases 0.3%; combined with the increased amount of air, this leads to leaner combustion and less soot production.

Fig. 7 illustrates the impact of ambient conditions on NO_x emissions, which decrease with increases in atmospheric temperature and humidity, and increase with increased pressure. Increasing the ambient temperature results in less air inducted into the cylinder, which must be balanced with increased fuel to maintain power. With the increase in temperature from 25 to 37°C, the mass of air in the cylinder decreases 2.8% and the fuel injected increases 0.9%, for a net decrease in the air–fuel ratio of 3.5% and a 1.6% increase in peak combustion temperature. While this results in increased soot, the reduction of excess oxygen from the richer combustion results in a decrease in NO_x. Increasing the relative humidity increases the specific heat capacity of the charge air, which leads to increased fuel delivery in order to maintain power. Specifically, a 0.5% increase in fuel injected is observed alongside a 1.2% decrease in the air–fuel ratio and a 25% decrease in NO_x as relative humidity increases from 10% to 90%. An increase in ambient pressure has a negligible impact on NO_x emissions because the wastegate on the turbocharger modulates to maintain a target boost pressure in the intake manifold. At both the lower and higher intake pressures, the intake manifold pressure is constant, but the pressure ratio across the compressor decreases 8.6% and the temperature in the intake manifold decreases 1.3% after the intercooler; the peak combustion temperature exhibits a 0.65% decrease and the pressure a 0.42% increase.

Fig. 8 demonstrates the effect of engine size and power output on the heat and emissions characteristics at three different environmental conditions. Increasing only the temperature results in an increase in heat output and soot, and a decrease in NO_x. Increasing ambient pressure has the opposite effect, reducing heat output and soot, and increasing NO_x. For comparably sized engines, a higher power output results in higher heat output. More fuel is required to achieve the higher power output, leading to increase in heat output. For engines with similar power ratings, the larger engine results in a higher heat output—in this case, with similar power and air–fuel ratio, the larger engine has a higher specific fuel consumption resulting from the greater charge volume. The smaller of the two engines achieves its power output with a higher boost pressure from the turbocharger. As a result, the smaller engine produces higher peak combustion temperature, leading to more NO_x production and less soot output.

Table 5
Conversion efficiency for diesel oxidation catalyst across all models and cases in this study compared to previous experimental studies.

	CO	Hydrocarbons
This study	100%	93%–97%
Wang et al. (2008)	100%	80%
Knafl et al. (2006)	100%	90%–95%
Sampara et al. (2008b)	100%	90%

The same trends are observed in these results as in the studies mentioned in the literature review. However, the NO_x emissions rates are above EPA Tier 2 limits because of the choice to fix the start of injection at the same point across all models. In reality, the injection timing can be retarded to decrease NO_x at the expense of increased soot. Ambient conditions and engine operation modes that increase NO_x also reduce soot: fuel-rich combustion, heterogeneous fuel–air mixtures, and/or lower combustion temperatures favor the production of soot; by contrast, fuel-lean combustion, homogeneous fuel–air mixtures, and higher combustion temperatures are favorable to the production of NO_x because of the excess air or the dissociation of diatomic nitrogen. Fuel consumption in all models is 2% to 23% higher than corresponding values in manufacturer specifications at the engine speed used in the simulation. The efficiency of the diesel oxidation catalyst in removing unburned hydrocarbons from the exhaust gas compares favorably to the results of experimental studies, as noted in Table 5. Diesel particulate matter is a combination of soot and unburned hydrocarbons, and, in these models, is reduced by removing unburned hydrocarbons. The one exception is the C15, which also includes a particulate filter to reduce soot output. Carbon monoxide is not considered in this study because the diesel oxidation catalyst removes it completely.

An industry partner provided a limited set of temperature and humidity measurements from an underground mine in an area with heavy-duty diesel machinery. One of the largest temperature changes was observed during a two-hour mucking activity with one loader and up to five trucks cycling through area. In the absence of working equipment, the conditions are 29°C dry-bulb, 80% relative humidity, and 103 kPa (baseline conditions). After two hours of engine operation,

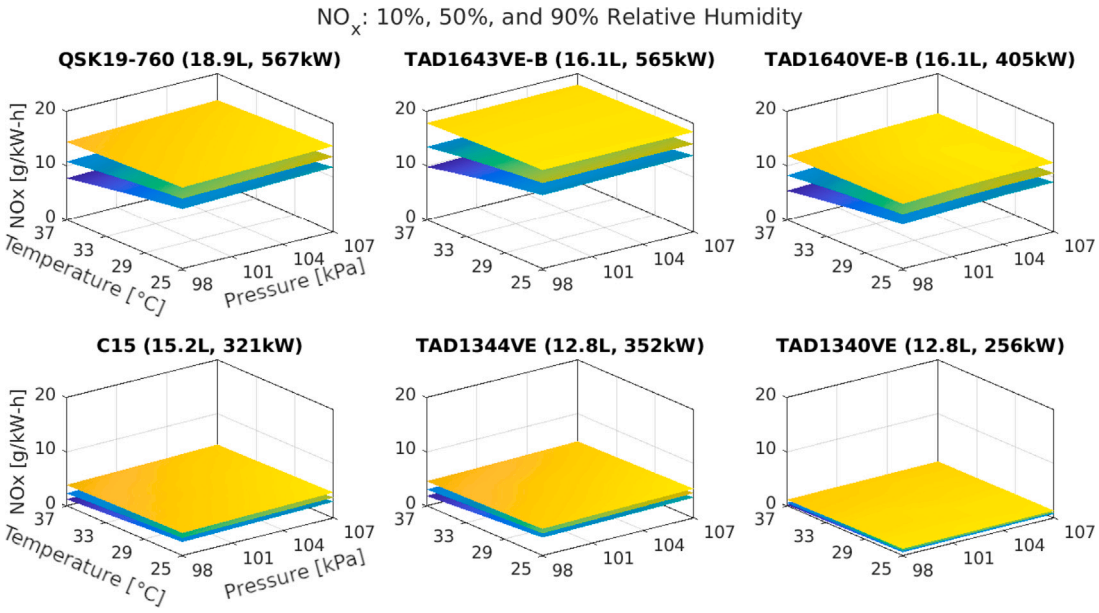

Fig. 7. Simulation results for each of the six engines depicted on each graph as one of three surfaces. Shown are NO_x outputs at 90% relative humidity (bottom surface), 50% relative humidity (middle surface), and 10% relative humidity (top surface). Note that the ordering of the surfaces is reversed relative to Figs. 5 and 6.

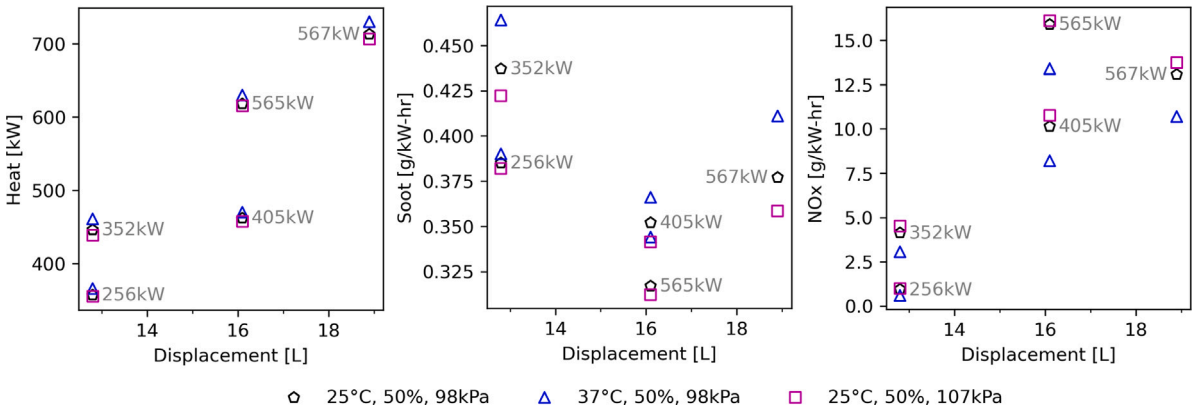

Fig. 8. A comparison of the engine size and power on heat, soot, and NO_x for various ambient conditions.

Table 6
Comparison of simulation results for ambient conditions corresponding to the starting (baseline) and peak temperature observed during a 2-hour period in an underground hard rock mine.

	Trucks			Loaders		
	QSK19	1643VE-B	1640VE	C15	1344VE	1340VE
Displacement (L)	18.9	16.1	16.1	15.2	12.8	12.8
Power output (kW)	567	565	405	305	352	256
Heat output rate at 100% load (kW)	719	624	464	402	450	363
Brake-specific soot (g/kW-h)	0.38	0.33	0.35	0.38	0.44	0.38
Brake-specific NO_x (g/kW-h)	11.1	13.4	8.55	2.56	3.32	0.62
Change in heat output rate relative to baseline (kW)	9	6	4	6	9	5
Change in soot relative to baseline (g/hW-h)	0.02	0.01	0.007	0.01	0.02	0.007
Change in NO_x relative to baseline (g/kW-h)	−0.75	−0.72	−0.50	−0.31	−0.37	−0.10
Change in heat output rate relative to baseline (%)	1.3	1.0	0.9	1.4	1.9	1.3
Change in soot relative to baseline (%)	5.2	4.2	2.0	2.5	4.0	1.9
Change in NO_x relative to baseline (%)	−6.8	−5.4	−5.8	−12.1	−11.1	−16.4

the temperature increases to a peak of 37°C dry-bulb with 60% relative humidity (peak-temperature conditions). This change in temperature corresponds to an average heat load of approximately 500 kW within the airway based on estimated ventilation parameters. The results of the engine simulations at the initial conditions are shown in Table 6. Baseline conditions are 28°C, 80% relative humidity, and 103 kPa, and the conditions at peak temperature are 37°C, 60% relative humidity, and 103 kPa. One loader is in the airway during the window, as well as one of five trucks. The top section of the table lists the engine specifications for each piece of equipment, the next section lists the

total heat (sensible and latent), soot, NO_x, and unburned hydrocarbon output; the one below lists the absolute change between the two conditions, and the last section lists the relative change. The changes observed are a result of increased fuel consumption, which produces more sensible and latent heat, and more soot and less NO_x due to the lower air–fuel ratio. Heat increases by 1.9% or less and soot increases by 5.2% or less for all the engines modeled, but the NO_x levels decrease between 5.4% and 16.4%. The impacts noted are due to changes in temperature and humidity because the ambient pressure remains the same; changes in temperature and relative humidity have the greatest impact on emissions within the range of parameters examined.

5. Conclusions

Simulations performed using the GT-SUITE software package on six engines demonstrate that ambient pressure, temperature, and humidity affect the soot, NO_x, and heat release rate. As mining operations continue to progress deeper underground, they can expect the heat and emissions produced by diesel engines to vary with ambient conditions. Assuming that they remain constant may lead to under- or over-estimation of the ventilation required.

The largest change observed during a working period is in NO_x, with up to a 16% decrease over the conditions examined. Changes in heat and soot output were lower at up to 1.9% and 5.2% increases, respectively. Results from this study show that the environmental conditions in underground mines can affect the performance of diesel equipment, with the changes in local temperature and relative humidity near heavy diesel equipment causing an increase in soot and a significant decrease in NO_x. As the emissions change due to local changes in the environment, temperature has a greater impact than humidity in the case observed. Pressure has no effect because it remains constant, but its effects may become pronounced as operations proceed deeper underground.

Results from this study are used in a medium-term, underground production scheduling model (Ogunmodede et al., 2022) that determines the best time to activate refrigeration in a mining operation, if necessary. Each activity is assigned a heat output value based on the equipment used to complete the activity. The inclusion of ventilation and refrigeration in a set of heat constraints ensures that the temperature in working areas remains within acceptable limits during each shift over the length of the schedule. In addition to the resource usage limits, this model includes a daily limit on the heat load determined by the maximum allowable temperature and the cooling capacity of the ventilation and refrigeration systems. As the initial temperature on each level is influenced by autocompression and the virgin rock temperature, the heat load assigned to an activity may vary based on the depth in the mine. For an activity to be scheduled on a particular day, its predecessor activities must be complete, and there must be sufficient resources available, e.g., drills, trucks, and cooling capacity. The resulting schedule maximizes net present value while ensuring that all activities can be completed with the available resources and without exceeding temperature thresholds. In addition to heat, results from this paper make it possible to include limits on other nuisances, such as soot or NO_x, in production scheduling models. Additional future work entails using these values in a short-term production scheduling model, solved at a finer time fidelity than the medium-term model, to track ambient conditions nearly real-time, thereby maintaining a safe work environment. Our results are derived under static conditions for use in an operational (but not necessarily real-time) production scheduling model; future research would therefore examine a dynamic setting in which input data fluctuates over time.

CRediT authorship contribution statement

Aaron Swift: Software, Investigation, Conceptualization, Methodology, Visualization, Writing, Data curation, Validation, Analysis. **Eric Smoorenburg:** Software, Investigation, Methodology, Visualization. **Alexandra Newman:** Conceptualization, Supervision, Methodology, Funding acquisition, Writing, Resources, Validation. **Gregory E. Bogin Jr.:** Conceptualization, Supervision, Methodology, Writing, Resources, Funding acquisition, Validation.

Declaration of competing interest

The authors declare that they have no known competing financial interests or personal relationships that could have appeared to influence the work reported in this paper.

Data availability

Data will be made available on request.

Acknowledgments

This research has been partially funded by the National Institute for Occupational Safety and Health, USA as part of the Mine Ventilation and Safety Research and Capacity Building program, contract number 0000HCCS-2019-36404. We would also like to thank our industry partner for its funding and support.

References

Abassi, A., Khalilarya, S., Jafarmadar, S., 2010. The influence of the inlet charge temperature on the second law balance under the various operating engine speeds in DI diesel engine. Fuel 89 (9), 2425–2432. http://dx.doi.org/10.1016/j.fuel.2010.04.034.

Bascompta, M., Castañón, A.M., Sanmiquel, L., Oliva, J., 2016. Heat flow assessment in an underground mine: an approach to improve the environmental conditions. DYNA 83 (197), 174–179. http://dx.doi.org/10.15446/dyna.v83n197.52182.

Breeze, P., 2018. Diesel engines. In: Breeze, P. (Ed.), Piston Engine-Based Power Plants. Academic Press, pp. 47–57.

Caterpillar, 2019. Cat C15 industrial diesel engine. https://emc.cat.com/pubdirect.ashx?media_string_id=SS-8895186-18396631-019.pdf.

Ceballos, J.J., Melgar, A., Tinaut, F.V., 2021. Influence of environmental changes due to altitude on performance, fuel consumption and emissions of a naturally aspirated diesel engine. Energies 14 (17), 5346. http://dx.doi.org/10.3390/en14175346.

Chen, S.K., Flynn, P.F., 1965. Development of a single cylinder compression ignition research engine. Technical Report, SAE Technical Paper.

Cummins, 2019. QSK19-G4 specification sheet. https://www.cummins.com/sites/default/files/2019-06/QSK19G4.pdf.

Cummins, 2020. KTA19-G4 specification sheet. https://mart.cummins.com/imagelibrary/data/assetfiles/0064182.pdf.

De la Vergne, J., 2014. Hard Rock Miner's Handbook, fifth ed. Stantec Consulting, Edmonton.

Dou, D., 2012. Application of diesel oxidation catalyst and diesel particulate filter for diesel engine powered non-road machines. Platin. Met. Rev. 56 (3), 144–154. http://dx.doi.org/10.1595/147106712X645466.

EPA, 2016. Integrated Science Assessment (ISA) for Nitrogen Dioxide - Health Criteria. U.S. Environmental Protection Agency (EPA), URL https://www.epa.gov/isa/integrated-science-assessment-isa-nitrogen-dioxide-health-criteria.

Gamma Technologies, 2017. GT-SUITE V2017. Gamma Technologies.

Hartman, H.L., Mutmansky, J.M., Ramani, R.V., Wang, Y.J., 1997. Heat sources and effects in mines. In: Mine Ventilation and Air Conditioning, third ed. Wiley, New York.

Heavy Duty Pros, 0000. Caterpillar Exhaust Valve, 1537024, https://www.heavydutypros.com/caterpillar-exhaust-valve-1537024.aspx.

Heavy Duty Pros, 0000. Caterpillar Intake Valve, 1537023, https://www.heavydutypros.com/caterpillar-intake-valve-1537023.aspx.

Heywood, J.B., 1988. Internal Combustion Engine Fundamentals. McGraw-Hill, New York.

Jääskeläinen, H., Khair, M.K., 2018. Valves and ports in Four-Stroke Engines. DieselNet https://dieselnet.com/tech/air_ports.php.

Juva, A., Zelenka, P., Tritthart, P., 1989. Influences of diesel fuel properties and ambient temperature on engine operation and exhaust emissions. SAE Trans. 98, 1–11.

Knafl, A., Busch, S.B., Han, M., Bohac, S.V., Assanis, D.N., Szymkowicz, P.G., Blint, R.D., 2006. Characterizing light-off behavior and species-resolved conversion efficiencies during in-situ diesel oxidation catalyst degreening. SAE Trans. 115, 53–62.

Lakshminarayanan, P.A., Aghav, Y.V., 2010. Modelling Diesel Combustion. Springer.

Lin, C.-Y., Jeng, Y.-L., 1996. Influences of charge air humidity and temperature on the performance and emission characteristics of diesel engines. J. Ship Res. 40 (02), 172–177. http://dx.doi.org/10.5957/jsr.1996.40.2.172.

Liu, S., Shen, L., Bi, Y., Lei, J., 2014. Effects of altitude and fuel oxygen content on the performance of a high pressure common rail diesel engine. Fuel 118, 243–249. http://dx.doi.org/10.1016/j.fuel.2013.10.007.

Maurya, T., Karena, K., Vardhan, H., Aruna, M., Raj, M.G., 2015. Potential sources of heat in underground mines–a review. Proc. Earth Planet. Sci. 11, 463–468. http://dx.doi.org/10.1016/j.proeps.2015.06.046.

Maximilien, D., Couture, C., Njanga, P.-E., Neesham-Grenon, E., Lachapelle, G., Coulombe, H., Hallé, S., Aubin, S., 2017. Diesel engine exhaust exposures in two underground mines. Int. J. Min. Sci. Technol. 27 (4), 641–645. http://dx.doi.org/10.1016/j.ijmst.2017.05.011.

Michael Donoghue, A., 2004. Heat illness in the U.S. Mining industry. Am. J. Ind. Med. 45 (4), 351–356. http://dx.doi.org/10.1002/ajim.10345.

Mohankumar, S., Senthilkumar, P., 2017. Particulate matter formation and its control methodologies for diesel engine: A comprehensive review. Renew. Sustain. Energy Rev. 80, 1227–1238. http://dx.doi.org/10.1016/j.rser.2017.05.133.

MSHA, 2023. Mine ventilation. In: Code of Federal Regulations. U.S. Department of Labor, Mine Safety and Health Administration (MSHA), Washington, D.C., URL https://www.ecfr.gov/current/title-30/chapter-I/subchapter-K/part-57/subpart-G/subject-group-ECFR06afab17eface73/section-57.8520.

Nogva, 0000. Cummins QSK19-M, http://www.nogva.no/download.aspx?object_id=1DAA2E487F4F41FBB1C9BCF5272750D6.pdf.

Norgate, T., Haque, N., 2010. Energy and greenhouse gas impacts of mining and mineral processing operations. J. Clean. Prod. 18 (3), 266–274. http://dx.doi.org/10.1016/j.jclepro.2009.09.020.

Ogunmodede, O., Lamas, P., Brickey, A., Bogin, G., Newman, A., 2022. Underground production scheduling with ventilation and refrigeration considerations. Optim. Eng. 23 (3), 1677–1705. http://dx.doi.org/10.1007/s11081-021-09682-4.

Paluchamy, B., Mishra, D.P., Panigrahi, D.C., 2021. Airborne respirable dust in fully mechanised underground metalliferous mines–Generation, health impacts and control measures for cleaner production. J. Clean. Prod. 296, 126524. http://dx.doi.org/10.1016/j.jclepro.2021.126524.

Pan, W., Yao, C., Han, G., Wei, H., Wang, Q., 2015. The impact of intake air temperature on performance and exhaust emissions of a diesel methanol dual fuel engine. Fuel 162, 101–110. http://dx.doi.org/10.1016/j.fuel.2015.08.073.

Pulkrabek, W.W., 2004. Engineering Fundamentals of the Internal Combustion Engine, second ed. Pearson Prentice Hall, Upper Saddle River, N.J.

Roghanchi, P., Kocsis, K.C., 2018. Challenges in selecting an appropriate heat stress index to protect workers in hot and humid underground mines. Saf. Health Work 9 (1), 10–16. http://dx.doi.org/10.1016/j.shaw.2017.04.002.

Sampara, C.S., Bissett, E.J., Assanis, D., 2008a. Hydrocarbon storage modeling for diesel oxidation catalysts. Chem. Eng. Sci. 63 (21), 5179–5192. http://dx.doi.org/10.1016/j.ces.2008.06.021.

Sampara, C.S., Bissett, E.J., Chmielewski, M., 2008b. Global kinetics for a commercial diesel oxidation catalyst with two exhaust hydrocarbons. Ind. Eng. Chem. Res. 47 (2), 311–322. http://dx.doi.org/10.1021/ie070813x.

Sasmito, A.P., Kurnia, J.C., Birgersson, E., Mujumdar, A.S., 2015. Computational evaluation of thermal management strategies in an underground mine. Appl. Therm. Eng. 90, 1144–1150. http://dx.doi.org/10.1016/j.applthermaleng.2015.01.062.

Turns, S.R., 2012. Chapter 5 - some important chemical mechanisms. In: An Introduction to Combustion: Concepts and Applications, third ed. McGraw-Hill, New York, pp. 149–182.

Volvo Penta, 2013a. Product bulletin TAD1340VE. https://pubs.volvopenta.com/publications/7749495.

Volvo Penta, 2013b. Product bulletin TAD1344VE. https://pubs.volvopenta.com/publications/7749499.

Volvo Penta, 2013c. Product bulletin TAD1640-1642VE-B. https://pubs.volvopenta.com/publications/47702906.

Volvo Penta, 2013d. Product bulletin TAD1643VE. https://pubs.volvopenta.com/publications/7749026.

Wagner Equipment Co., June 20, 2022. Personal communication.

Wang, T.J., Baek, S.W., Lee, J.-H., 2008. Kinetic parameter estimation of a diesel oxidation catalyst under actual vehicle operating conditions. Ind. Eng. Chem. Res. 47 (8), 2528–2537. http://dx.doi.org/10.1021/ie071306i.

Widiatmojo, A., Sasaki, K., Sugai, Y., Suzuki, Y., Tanaka, H., Uchida, K., Matsumoto, H., 2015. Assessment of air dispersion characteristic in underground mine ventilation: Field measurement and numerical evaluation. Process. Saf. Environ. Prot. 93, 173–181. http://dx.doi.org/10.1016/j.psep.2014.04.001.

Yeoman, K., DuBose, W., Bauerle, T., Victoroff, T., Finley, S., Poplin, G., 2019. Patterns of heat strain among a sample of US underground miners. J. Occup. Environ. Med. 61 (3), 212–218. http://dx.doi.org/10.1097/JOM.0000000000001518.

Yeoman, K., Weakley, A., DuBose, W., Honn, K., McMurry, T., Eiter, B., Baker, B., Poplin, G., 2022. Effects of heat strain on cognitive function among a sample of miners. Appl. Ergon. 102, 103743. http://dx.doi.org/10.1016/j.apergo.2022.103743.

Zhu, D., Nussbaum, N.J., Kuhns, H.D., Chang, M.-C.O., Sodeman, D., Moosmüller, H., Watson, J.G., 2011. Real-world PM, NOx, CO, and ultrafine particle emission factors for military non-road heavy duty diesel vehicles. Atmos. Environ. 45 (15), 2603–2609. http://dx.doi.org/10.1016/j.atmosenv.2011.02.032.